Journal of Applied Fluid Mechanics, Vol. 17, No. 7, pp. 1524-1535, 2024.
Available online at www.jafmonline.net, ISSN 1735-3572, EISSN 1735-3645.
https://doi.org/10.47176/jafm.17.7.2341

Numerical Simulation of Inlet Void Fraction Affecting Oil-gas Two-phase Flow Characteristics in 90° Elbows

W. Sha[1†], G. Leng[2], R. S. Xu[1] and S. Li[3]

[1] *School of Aero-engine, Shenyang Aerospace University, Shenyang, Liaoning, 110136, China*
[2] *Key Laboratory of Power Transmission Technology on Aero-engine, aero-engine corporation of China, Shenyang, Liaoning, 110066, China*
[3] *Shenyang Medical College, Shenyang, Liaoning, 110136, China*

†Corresponding Author Email: shawei@stu.sau.edu.cn

ABSTRACT

Air can have an adverse effect on the performance of an aero-engine lubrication system. A numerical analysis was conducted to explore the influence of inlet void fraction and pipe layout on the characteristics of oil-gas two-phase flow in a 90° elbow. The pipes were arranged horizontally and vertically with inlet void fractions of 0.05-0.15. The laws governing flow velocity, void fraction, and pressure along the pipe were determined separately. The results revealed the formation of large-scale vortices with high gas volume fractions inside both types of elbows, which exacerbate oil-gas separation and cause additional head loss. The maximum pressure drop was observed at approximately one pipe diameter downstream of the elbow outlet, which initially increases with the inlet void fraction and then gradually stabilizes. Asymmetric secondary flow vortices in the horizontal elbow were found to enhance oil-gas separation and accelerate lubricating oil to greater extent than in a vertical elbow under the same conditions. Consequently, the maximum pressure drop caused by flowing through the horizontal elbow is higher than that in the vertical elbow.

Article History

Received September 27, 2023
Revised January 26, 2024
Accepted February 8, 2024
Available online April 30, 2024

Keywords:

Acceleration effect
Gravity effect
Bubbly flow
Head loss
Slip ratio
Void fraction

1. INTRODUCTION

During the operation of an aero-engine, inevitable mixing of air in the lubrication system leads to the formation of an oil-gas two-phase flow within the pipes. The physical properties and flow characteristics of the oil-gas mixture differ significantly from those of pure lubricant, directly impacting the efficiency of the lubrication system (Flouros et al., 2015, 2016). Given the numerous elbows in the lubrication system, it becomes imperative to fully understand the characteristics of oil-gas flows inside these components in order to ensure effective lubrication performance.

Gas-liquid two-phase flow problems are a persistent concern among scholars and engineers, including crucial research topics such as flow regime, pressure drop, and void fraction (Qiao et al., 2017; Kong et al., 2018). Experimentation offers a direct means of observing flow regimes and optimizing theoretical models (Zubir et al., 2019; Fang et al., 2020). With advancements in computer technology, computational fluid dynamics (CFD) simulations have emerged as a useful and cost-effective research tool (Atif & Senouci, 2019; Yayla et al., 2019; Yang et al., 2022).

Existing research findings emphasize the significant impact of elbows on void fraction distributions. Qiao and Kim (2016, 2018), for example, found that the void distribution exhibits a bimodal-to-bimodal or a bimodal-to-single-peaked characteristic region when a bubbly flow vertically flows upward through the elbow at different superficial gas velocities. Ogunsesan et al. (2021) found that a vertical-upward churn flow transforms into a wavy stratified flow in the horizontal section after a 90° bend. The flow regime and slug frequency of a slug flow did not change after passing through the elbow, but the void fraction increased along the pipe (Bressani & Mazza, 2018; Ogunsesan et al., 2021). Liu et al. (2015) attributed changes in void fractions and flow regimes to the floating and gathering of bubbles in a 90° bend, resulting in an overall rotational bubble due to uneven velocity distributions along the cross-section perpendicular to the axis. Asymmetrical secondary flows were observed in both horizontal and vertical bends. Chen et al. (2019) observed a kidney-bean shaped void distribution when the average void fraction ranged from 15% to 30%, covering flow regimes from

NOMENCLATURE

D	pipe diameter
f_{drag}	drag function
G_k	turbulent kinetic energy due to mean velocity gradients
G_b	turbulent kinetic energy due to mean buoyancy
Li	length of upstream straight pipe
Lo	length of downstream straight pipe
S_{RC}	coalescence sink term
S_{TI}	breakage source term
α_g	volume fraction of gas
α_i	Inlet void fraction
α_k	volume fraction of phase k
$\Delta\alpha$	maximum void fraction compared to the inlet
$(\Delta v_h)_{4\text{-}6}$	flow velocity of lubricating oil between Surface-4 and Surface-6 in horizontal elbow
$(\Delta v_v)_{4\text{-}6}$	increment in flow velocity of lubricating oil between Surface-4 and Surface-6 in vertical elbow
$\lvert\Delta S_h\rvert_{4\text{-}6}$	changes in slip ratio between Surface-4 and Surface-6 in horizontal elbow
$\lvert\Delta S_v\rvert_{4\text{-}6}$	changes in slip ratio between Surface-4 and Surface-6 in vertical elbow
$(\Delta v_h\text{-}\Delta v_v)_{4\text{-}6}$	difference between $(\Delta v_h)_{4\text{-}6}$ and $(\Delta v_v)_{4\text{-}6}$
$(\Delta S_h\text{-}\Delta S_v)_{4\text{-}6}$	difference in slip ratio between two types of pipes
Δp	total pressure drop in elbow
$\Delta p_{\max}$	maximum pressure drop of mixture flowing through elbow
$(\rho_v\text{-}\rho_h)_6$	density difference between vertical elbow and horizontal elbow at Surface-6
μ_m	viscosity of mixture
$\vec{v}_m$	mass-averaged velocity of mixture
ρ_m	density of mixture
σ_k	turbulent Prandtl numbers for k
σ_ε	turbulent Prandtl numbers for ε
τ_g	bubble relaxation time
χ_g	interfacial area concentration

dispersed to slug flows. The void fraction of a bubbly flow increases downstream of a 90° bend, since the bubble move in the opposing direction of the deflection-inertia force caused by the bend, leading to bubble breakage and coalescence (Dang et al., 2018; Pour et al., 2018). Additionally, the intensity of eddies and the superficial velocity of water and air both impact the void fraction distribution downstream and upstream of an elbow (Bowden et al., 2018; Zahedi et al., 2022).

Reducing head losses in pipes is a critical aspect of designing lubrication systems for aviation engines. Elbows, typical sources of local loss in pipes, contribute significantly to this design challenge. For gas-liquid two-phase flows, an increase in liquid or gas velocity causes the local pressure loss in an elbow to increase (Qiao & Kim, 2016). The classification of flow regimes in oil-gas two-phase flows is similar to that of gas-water two-phase flows (Debnath et al., 2015; Ban et al., 2018; Kim & Kim, 2022). However, the higher viscosity of lubricating oil renders the flow mechanisms and parameter change laws from gas-water mixtures inapplicable to oil-air mixtures (Al-Safran & Al-Qenae, 2018; Li et al., 2022). To date, investigations into two-phase flow regimes and pressure drop in oil-gas mixtures have mainly focused on straight pipes. There have been few detailed investigations on 90° elbows.

As aero-engine technologies continue to advance, the demand for extensive flow data in pipes has intensified. The temporal and cost advantages of CFD simulations have thus grown increasingly prominent. To the best of the author's knowledge, this study represents the first numerical analysis of the effects of inlet void fraction on the flow characteristics of aviation lubricating oil-air bubbly flow in a 90° elbow. The inlet void fraction (α_i) is defined as the volume fraction of gas at the inlet.

Three novel contributions of this study have been summarized as follows. (1) A two-fluid Euler approach was established with sufficient stability and resolution that can describe the slip velocity between lubricating oil and air. This approach was validated by comparison against physical engine test results. (2) The inlet void fraction and the velocity of lubricating oil were aligned with the general operating conditions of aviation engines. (3) The position of the maximum pressure drop was observed, as well as the changes in pressure drop with different inlet void fractions in a 90° elbow under the coupling effect of gravity and oil-gas separation. This analysis hinged on flow field, pressure field, and slip ratio characteristics. The results of this work reveal various characteristics of flow fields and local head losses in oil-air two-phase flows, specific to elbows, providing valuable insights for the design of pipes in lubrication systems.

2. MODELLING METHODOLOGY

2.1 Basic Assumptions

Lubricating oil flows rapidly in pipes. The oil has a slight temperature difference with its environment during engine operation, and thus can be approximated as an adiabatic flow. The conditions at inlet and outlet of the pipe are basically stable, and the fluid inside the pipe does not exchange heat or work with the environment. Consequently, the fluid is a stable flow. In actual working conditions, the gas doped in the lubricating oil inside pipes is composed mostly of fine bubbles with

relatively low gas content, so a homogeneous model is applicable.

2.2 Governing Equations

A steady-state mixture model based on an assumed homogeneous flow was adopted in this study. This model includes a continuity equation, momentum equation, energy equation, volume fraction equation, and slip velocity equation for oil-gas mixtures. It is suitable for bubbly flows with low gas volume fractions. The control equation is as follows:

(1) Continuity equation

$$\nabla\cdot\left(\rho_m\vec{v}_m\right)=0 \tag{1}$$

where ρ_m and $\vec{v}_m$ are the density and mass-averaged velocity of the mixture, respectively.

(2) Momentum equation

$$\begin{aligned}&\nabla\cdot\left(\rho_m\vec{v}_m\vec{v}_m\right)=-\nabla p+\nabla\cdot\left[\mu_m\left(\nabla\vec{v}_m+\nabla\vec{v}_m^T\right)\right]\\&+\rho_m\vec{g}+\vec{F}-\nabla\cdot\left(\sum_{k=1}^{2}\alpha_k\rho_k\vec{v}_{dr,k}\vec{v}_{dr,k}\right)\end{aligned} \tag{2}$$

where μ_m is the viscosity of the mixture; α_k, ρ_k and $\vec{v}_{dr,k}$ are the volume fraction, density and drift velocity of phase *k*, respectively and $\vec{F}$ is a body force.

(3) Volume fraction equation

$$\nabla\cdot(\alpha_g\rho_g\vec{v}_m)=-\nabla\cdot(\alpha_g\rho_g\vec{v}_{dr,g})+\dot{m}_g \tag{3}$$

where α_g and ρ_g are the volume fraction and density of the gas phase; $\dot{m}_g$ is the mass transfer between the gas and liquid.

(4) Slip velocity equation

The slip velocity is the velocity of the gas phase (*g*) relative to the velocity of the liquid phase (*l*):

$$\vec{v}_{gl}=\frac{\tau_g}{f_{drag}}\frac{\left(\rho_g-\rho_m\right)}{\rho_g}\vec{\alpha} \tag{4}$$

where τ_g is the bubble relaxation time, $\vec{\alpha}$ is the bubble acceleration, and f_{drag} is the drag function proposed by Schiller and Naumann (1935):

$$f_{drag}=0.0183\mathrm{Re}\qquad \mathrm{Re}>1000 \tag{5}$$

(5) Interfacial area concentration equation

By using this equation, the interfacial area between the gas and liquid can be calculated as follows:

$$\nabla\cdot\left(\rho_g\vec{u}_g\chi_g\right)=\frac{2}{3}\frac{\dot{m}_g}{\alpha_g}\chi_g+\rho_g\left(S_{RC}+S_{TI}\right) \tag{6}$$

where χ_g is the interfacial area concentration, $\dot{m}_g$ is the mass transfer rate into the gas phase per unit mixture volume, S_{RC} is the coalescence sink term owing to random collision, and S_{TI} is the breakage source term owing to turbulent impact.

(6) Turbulence model

The realizable *k*-*ε* model with enhanced wall treatment was used in this study. This model performs well for analyzing swirling and boundary layer flows under strong adverse pressure gradients, as well as complex secondary flows. The transport equations for *k* and *ε* in the realizable *k*-*ε* model are:

$$\frac{\partial}{\partial x_i}(\rho k u_i)=\frac{\partial}{\partial x_j}\left[\left(\mu+\frac{\mu_t}{\sigma_k}\right)\frac{\partial k}{\partial x_j}\right]+G_k+G_b-\rho\varepsilon-Y_M \tag{7}$$

and

$$\begin{aligned}&\frac{\partial}{\partial x_i}(\rho\varepsilon u_i)=\frac{\partial}{\partial x_j}\left[\left(\mu+\frac{\mu_t}{\sigma_\varepsilon}\right)\frac{\partial\varepsilon}{\partial x_j}\right]+\rho C_1 S\varepsilon\\&-\rho C_2\frac{\varepsilon^2}{k+\sqrt{\nu\varepsilon}}+C_{1\varepsilon}\frac{\varepsilon}{k}C_{3\varepsilon}G_b\end{aligned} \tag{8}$$

where $C_1=\max\left(0.43,\frac{\eta}{\eta+5}\right)$, $\eta=S\frac{k}{\varepsilon}$, $S=\sqrt{2S_{ij}S_{ij}}$, G_k and G_b denote the generation of turbulent kinetic energy due to the mean velocity gradient and buoyancy, respectively. Y_M represents the effect of the fluctuating dilatation in compressible turbulence on the overall dissipation rate. $C_{1\varepsilon}$ =1.44, C_2 =1.9. σ_k (=1.0), and σ_ε (=1.2) are the turbulent Prandtl numbers for *k* and *ε*, respectively.

2.3 Computation Scheme and Conditions

A steady-state pressure-based solver in ANSYS Fluent was utilized to solve the governing equations. The pressure-velocity coupling method was SIMPLE, with the least squares cell-based used to compute the gradient terms. PRESTO! was used to discretize the pressure term and a second-order upwind scheme was used to discretize other control equations. The convergence criterion for all equations was 1.0×10^{-3}. The primary phase and secondary phase were 4010 lubricating oil and air, respectively, with same reference temperature of 70℃. The physical properties of oil and air are listed in Table 1.

2.4 Model Validation

The model was validated against the results of an experiment investigating two-phase flow pressure drop across 90° elbows (Qiao & Kim, 2018). In the experiment, a mixture was pumped into a vertical-upward elbow with liquid velocity of 4 m/s and gas velocity of 0.87 m/s. The experimental section can be approximated as insulated tube without phase transition. As shown in Fig. 1, the

Table 1 Physical properties of oil and air

Parameters	Materials	
	4010 oil	Air
Density / (kg/m^3)	959.96	1.02
Viscosity / (Pa·s)	7.70×10^{-3}	2.04×10^{-5}
Specific heat / (J/kg/k)	1845.0	1008.5
Thermal conductivity / (W/m/k)	0.145	0.029
Surface tension /(N/m)	0.021	/

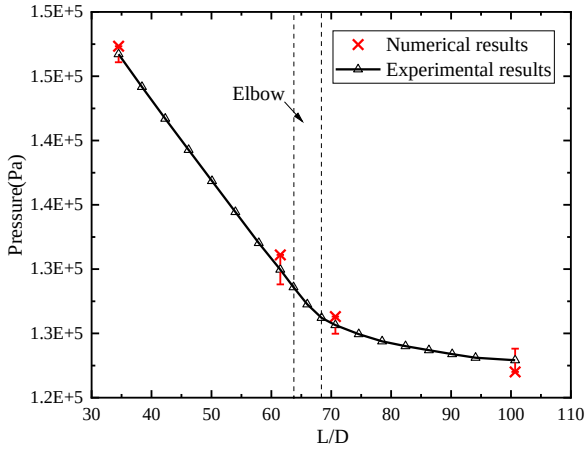

Fig. 1 Validation of numerical model

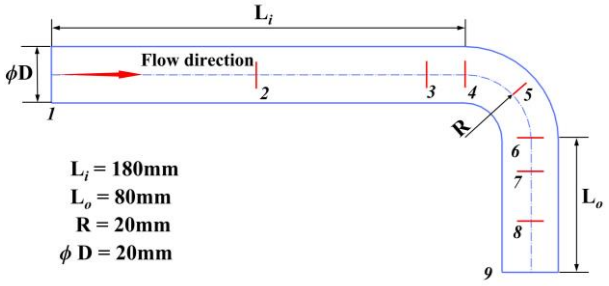

Fig. 2 Pipe geometric dimensions

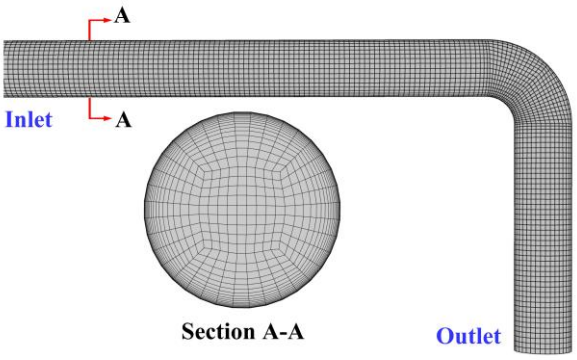

Fig. 3 Pipe grid

simulation results closely aligned with the experiment data in terms of the pressure along the tube, and the error does not exceed 1%.

3. GEOMETRIC MODEL AND MESH

A 90° elbow, which is commonly used in aviation-engine oil systems, was adopted in this study. The geometric dimensions of a horizontal elbow and vertical elbow are similar. As shown in Fig. 2, the diameter of the whole pipe is ϕD=20 mm; the elbow is connected to two straight pipes with lengths of 180 mm (L*i*) and 80 mm (L*o*), respectively, to ensure the full development of liquid flow upstream and downstream of the elbow. As

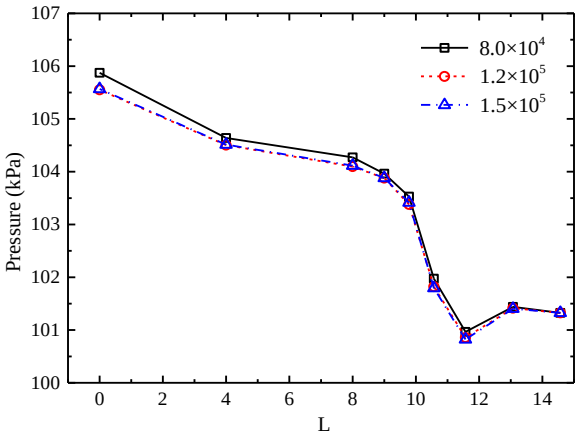

Fig. 4 Comparison of pressure along pipe calculated with three grid numbers

shown in Fig. 3, hexahedron grids and O-shaped layout were adopted to divide the three-dimensional pipe. The grids at the boundary layer were densified and the height of the first-layer grid was set to 0.02 mm. The growth rate of the grid is 1.2 and the maximum y-plus of the grid is 2.03.

A horizontal elbow with inlet void fraction (α_i) of 0.10 and flow velocity of 3.03m/s was adopted to verify the grid independence. The pressure along the pipe, calculated using three different numbers of grids, is depicted in Fig. 4. The *L* in this figure and throughout the remainder of this paper denotes a dimensionless length equal to that the true length divided by the diameter of the pipe. As the grids increased from 8.0×10^4 to 1.2×10^5, the pressure along the pipe decreased to varying extent. As the grids increased further to 1.5×10^5, there was no apparent change in pressure. The number of grids used in subsequent analyses was 1.2×10^5.

4. RESULTS AND DISCUSSION

4.1 Calculation Conditions

An oil-gas two-phase flow in an elbow was simulated under different inlet void fraction conditions, as discussed in detail in this section. The conditions of the numerical simulation are described in Table 2. When designing an engine lubrication system, α_i=0.05-0.15 are typical empirical values. A stable velocity inlet with turbulence intensity of 5% was used as the upstream flow of the elbow in this simulation. The pressure at the pipe outlet was set to 101325 Pa for all cases. The tube wall was a non-slip insulated wall, and the gravitational acceleration was 9.81m/s^2 along the y-direction. Nine surfaces for monitoring data were established perpendicular to the central axis in the pipe, as marked by the red straight line in Fig. 2.

Surface-4 and Surface-6 are the inlet and outlet of the elbow, respectively. The distances between each monitoring surface and the inlet are listed in Table 3. The average value of each monitoring surface was employed as the result at the corresponding surface.

Table 2 Calculation conditions for each case

Case	Pipe direction	Inlet velocity (m/s)	Reference temperature (℃)	Inlet void fraction	Inlet pressure (Pa)
1	Horizontal	3.03	70	5%	101325
2				10%	
3				15%	
4	Vertical	3.03	70	5%	101325
5				10%	
6				15%	

Table 3 Location of monitoring surface

Order number	1	2	3	4	5	6	7	8	9
Distance *l* (mm)	0	80	160	180	196	211	231	261	291
Dimensionless distance *L*(*l*/*D*)	0.00	4.00	8.00	9.00	9.79	10.58	11.57	13.07	14.57

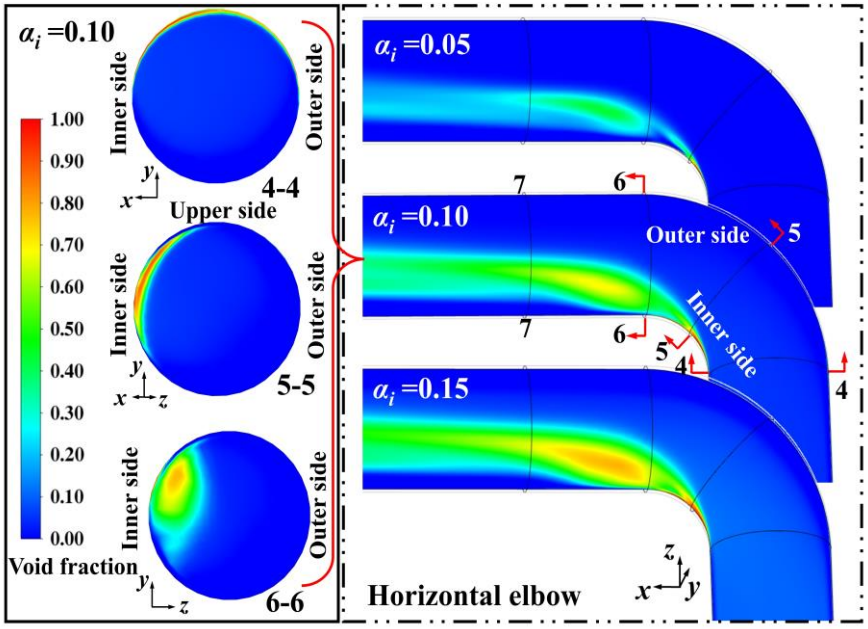

Fig. 5 Contour map of void fraction on longitudinal section (x-z plane) of horizontal elbows with different α_i, on surface-4, -5, and -6 at α_i =0.10

4.2 Void Fractions in Pipes

Figure 5 and Fig. 6 show contour maps of void fractions in horizontal and vertical elbows, respectively. In the cross-section, the gas in the horizontal pipe rises to the top wall before entering the elbow, while the oil and gas in the vertical pipe remain generally well-mixed. A vertical view revealed that, within the elbow, air separates from the lubricating oil on the inner side of the elbow in both pipe directions. The area of oil-gas separation extends downstream and gradually expands in volume. The key distinction between these two cases is the symmetrical distribution of gas in the vertical elbow, while the gas in the horizontal elbow is distributed more above the pipe due to the influence of gravity.

Comparing these contour maps under different conditions revealed that an increase in α_i results in a larger volume of air in both pipe layouts. When α_i values are equal, the volume of the area for oil-gas separation inside horizontal elbow is larger, signifying more pronounced oil-liquid separation. The underlying reason for this observation can be analyzed according to the flow field. Figure 7 provides a comparison of void fractions along the path of two types of pipes. In both cases, the void fraction slightly decreases before oil and gas enter the elbow. After passing through the 45° corner, the void fraction quickly increases, continually increasing until downstream straight pipe section with a length equal to the pipe diameter, at which point it gradually decreases to restore to inlet void fraction. The elevation in maximum void fraction compared to the inlet ($\Delta\alpha$) increases with α_i in both cases. When the α_i value is constant, the void fraction downstream of the horizontal elbow is higher than that downstream of the vertical elbow, indicating that the separation between oil and gas after flowing through a horizontal elbow is more severe. This void fraction trend is consistent with that displayed in the contour map.

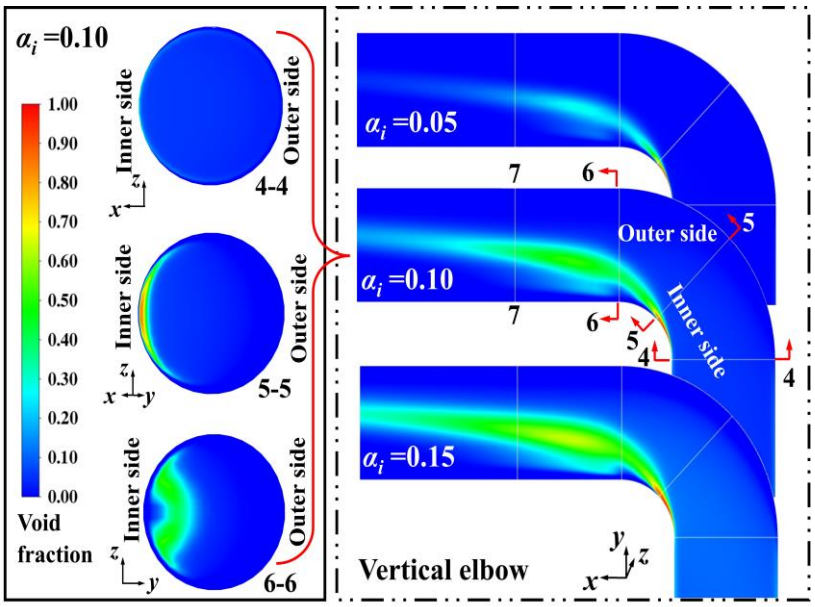

Fig. 6 Contour map of void fraction on longitudinal section (x-y plane) of vertical elbows with different α_i, on surface-4, -5, and -6 at α_i =0.10

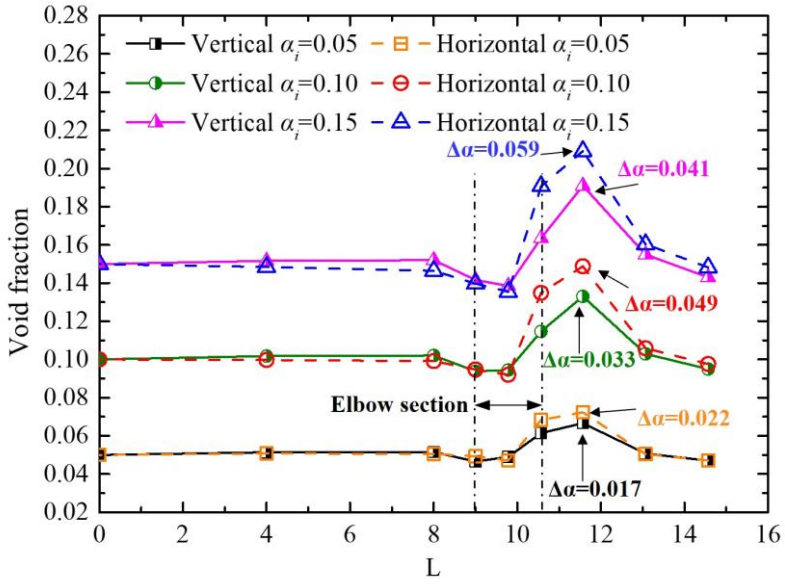

Fig. 7 Changes in void fraction along pipe path

4.3 Flow Characteristics in Pipes

Figure 8 and Fig. 9 display velocity-vector maps with three different α_i values in horizontal and vertical elbows, respectively, with the same coordinate systems as those shown in Fig. 5 and Fig. 6. From the vertical view, the oil-gas flow in both horizontal and vertical pipe are stable before entering the elbow. In the elbow, the axial flow velocity along the inner side is significantly higher than that along the outer side under the influence of deflection-inertia force.

As a result of fluid continuity, the flow velocity along the outer side is greater than that along the inner side of the pipe after the mixture passes though the 45° corner. A vortex area extending to the vicinity of Surface-7 forms on the inner side of the elbow due to the separation of boundary layer. Surfaces-4, -5, and -6 show a symmetrical secondary flow forming in the vertical elbow, while the secondary flow in the horizontal elbow is more inclined towards the upper wall.

Changes in α_i did not significantly impact the flow field. Comparison with Fig. 5 and Fig. 6 reveals that the distribution of the vortex area closely overlaps with that of the high-void-fraction zone. In theory, the density and inertia force of air are much smaller than that of lubricating oil, and it is more susceptible to the influence of gravity direction and flow disturbances. The calculation results indicate that large-scale low-speed vortices in the elbow are prone to oil-gas separation, and that asymmetric and strong vortices caused by secondary flow exacerbate this phenomenon. This is why the void fraction in the horizontal elbow is higher than that in the vertical elbow.

Figure 10 and Fig. 11 illustrate the flow velocities of lubricating oil and air along both pipe paths. As shown in

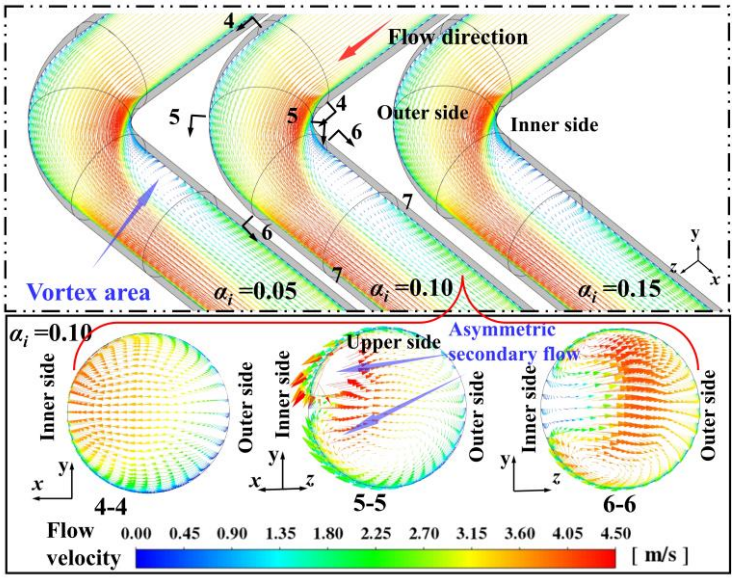

Fig. 8 Flow field of horizontal elbow with different α_i

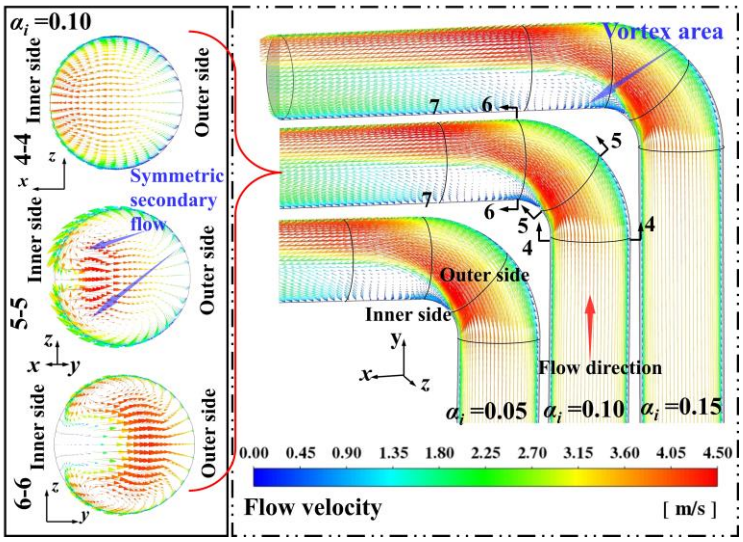

Fig. 9 Flow field of vertical elbow with different α_i

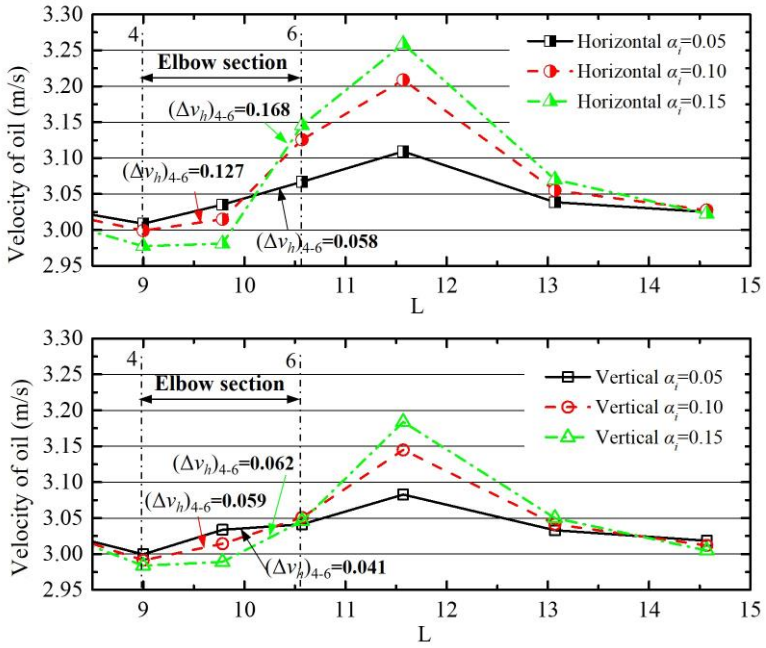

Fig. 10 Mean velocity of lubricating oil along pipe path with different α_i

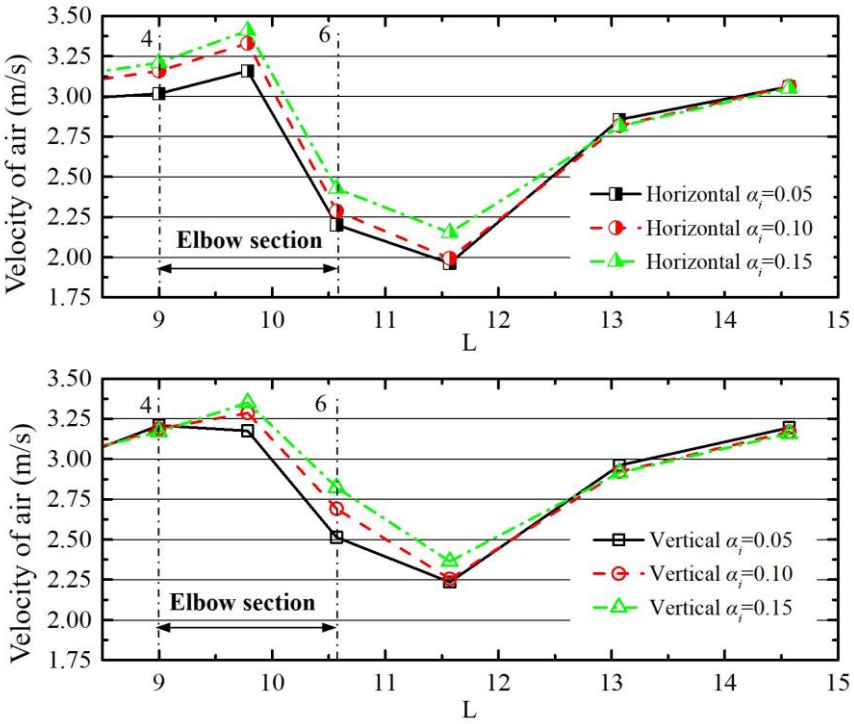

Fig. 11 Mean velocity of air along pipe path with different α_i

Fig. 10, the flow area of oil decreases due to a gradual increase in void fraction after the mixture enters the two types of elbows. Based on fluid continuity principles, the velocity of lubricating oil gradually increases until peaking at approximately 1D downstream from the elbow (represented by $u_{l,max}$). Subsequently, due to the gradual decrease in void fraction, the velocity of lubricating oil gradually decreases along the pipe path.

As shown in Fig. 7, for both types of pipes, $\Delta\alpha$ increases and the corresponding flow area of oil decreases as α_i increases, which lead to an increase in $u_{l,max}$. At the same time, as α_i increases, the difference in the velocity of lubricating oil between Surface-4 and Surface-6 in the horizontal elbow (represented by $(\Delta v_h)_{4\text{-}6}$) increases from 0.058 to 0.168, while that in the vertical elbow (represented by $(\Delta v_v)_{4\text{-}6}$) increases from 0.041 to 0.062. To this effect, increasing the inlet void fraction intensifies the lubricating oil acceleration effect in the elbow. This phenomenon is not obvious in a vertical elbow but more pronounced in a horizontal elbow.

Under the same α_i, the velocity of lubricating oil at the outlet and the acceleration effect generated by the flow through the horizontal elbow are greater than those in the vertical elbow. This is because a mixture with larger void fraction is generated in a horizontal elbow compared to a vertical elbow.

With reference to Fig. 11 and Fig. 7, the air velocity and the void fraction exhibit an inverse correlation with changes in flow area. In both types of pipes, the mean velocity of air increases slightly after the two-phase flow enters the elbow and peaks at the 45° corner (represented by $u_{g,max}$). Subsequently, a vortex area dominated by air forms on the inner side of the elbow with a significant decrease in mean velocity of air. The air velocity decreases to its minimum at about 1D downstream from the elbow (represented by $u_{g,min}$), followed by gradual acceleration along the pipe path. In the same type of pipe, the mass flow rate of air increases with α_i, while $u_{g,max}$ and $u_{g,min}$ also increase. Under the same α_i and flow velocity, the mean velocity and $u_{g,min}$ of air are greater after flowing out of the vertical elbow than the horizontal elbow due to the smaller void fraction in the vertical elbow.

4.4 Local Head Loss in Pipes

Figure 12 illustrates the slip ratio along the pipe path for two types of elbows at different α_i values. The slip ratio represents the ratio of the air velocity to the lubricating oil velocity. As shown in this figure, the slip ratio of the two-phase flow reaches its maximum at the 45° corner in both types of pipes, then sharply decreases toward its lowest value at approximately 1D downstream from the elbow. From there, it gradually increases and recovers to about 1.0 at three times the pipe diameter. It seems that gas-liquid separation is most severe at the 45° corner and the outlet, which is consistent with the gas-liquid contour map.

The changes in slip ratio between Surface-4 and Surface-6 in horizontal and vertical elbows are denoted by $|\Delta S_h|_{4\text{-}6}$ and $|\Delta S_v|_{4\text{-}6}$, respectively. The $|\Delta S_h|_{4\text{-}6}$ value increases from 0.285 to 0.321 and then decreases to 0.307 while $|\Delta S_v|_{4\text{-}6}$ decreases from 0.244 to 0.135 as α_i increases. An increase in the amplitude of change in slip ratio along a pipe indicates an increase in frictional head loss (Chisholm, 1980). Under the same α_i, the slip ratio at the outlet of the horizontal elbow deviates significantly from 1.0 compared to the vertical elbow, which further indicates that the acceleration effect of lubricating oil flowing through a horizontal elbow is greater than that through a vertical elbow.

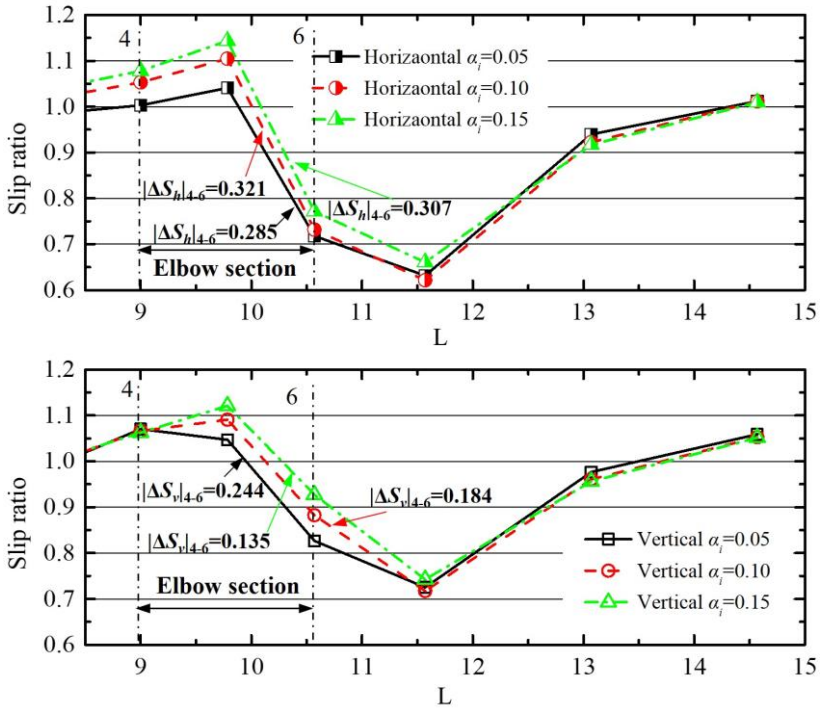

Fig. 12 Slip ratio along pipe path with different α_i

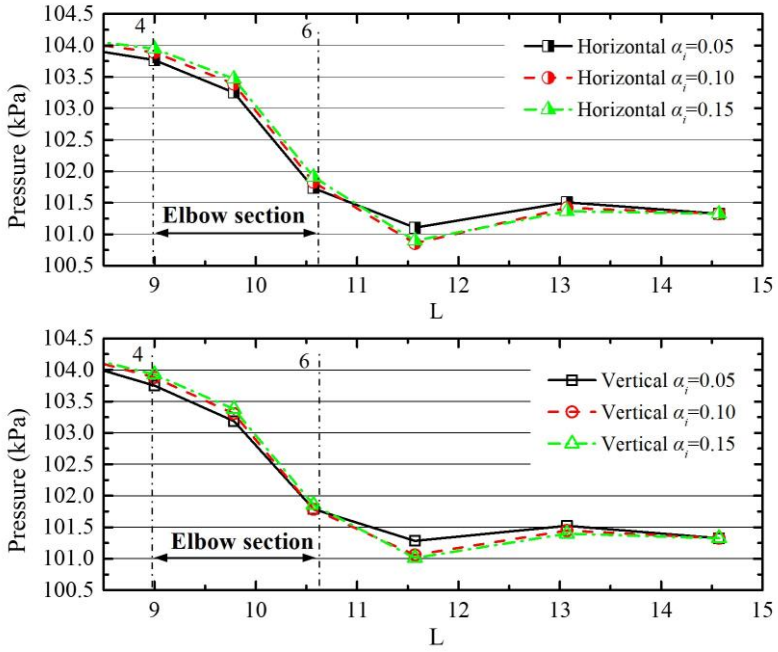

Fig. 13 Static pressure along pipe path with different α_i

Figure 13 shows the changes in static pressure (shortened here simply to "pressure") inside the pipe. The pressure within both types of pipes rapidly decreases after the mixture enters the elbow and continues to decrease until reaching its minimum at approximately 1D downstream from the elbow, which is consistent with the location exhibiting the lowest slip ratio and the highest velocity of lubricating oil in previous analyses. After passing through this position, the pressure slightly increases due to a decline in the vortex, then gradually decreases along the straight pipe. An increase in the oil velocity significantly increases the turbulence degree and flow resistance, and the influence of the velocity difference between the oil and gas on the frictional head loss grows more significant as this difference increases.

As shown in Fig. 14, Δp (Δp=p_4-p_6) is the total pressure drop in the elbow and Δp_{max} (Δp_{max}= p_4-p_7) is the maximum pressure drop of the mixture flowing through the elbow. For both types of elbows, when α_i increases from 0.05 to 0.1, Δp slightly increases; as α_i continues to rise to 0.15, the change in Δp is very small. The Δp_{max} value gradually increases with α_i, but the amplitude of the increase gradually decreases. Under the conditions of α_i=0.10 and α_i=0.15, the Δp in the vertical elbow is greater than that in the horizontal elbow. When

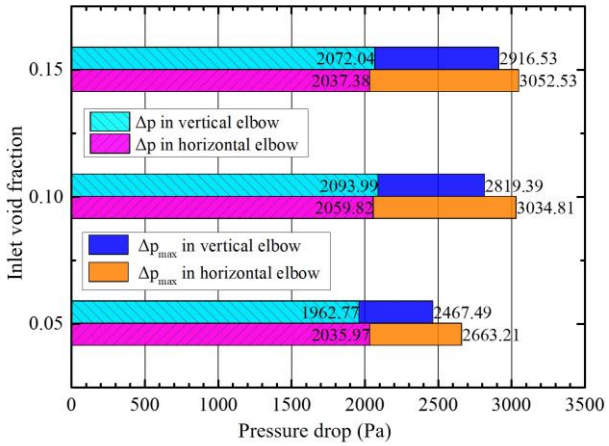

Fig. 14 Pressure drop in an elbow with different α_i

α_i=0.05, the Δp value is larger in the horizontal elbow. Under the three working conditions tested, the Δp_{max} value is consistently greater in the horizontal elbow than the vertical elbow.

The total pressure drop of gas-liquid two-phase flow in a pipe includes three parts: gravity pressure drop, acceleration pressure drop, and friction pressure drop corresponding to frictional head loss. The simulation results of this study indicate that the acceleration effects of oil in both elbows increase with α_i, which causes an increase in acceleration pressure drop. Simultaneously, the friction pressure drop in the horizontal elbow first increases and then decreases as α_i increases, while the friction pressure drop in the vertical elbow decreases as α_i increases. The increase in α_i causes a decrease in the density of the mixture. Accordingly, the magnitude of the change in gravity pressure drop also decreases under the same change in height. Under the combined effect of these three types of pressure drops, the total and maximum pressure drops within both types of elbows do not increase infinitely with α_i, but instead gradually tend toward stability.

As shown in Table 4, an increase in α_i causes several distinct changes.

(1) The difference between $(\Delta v_h)_{4\text{-}6}$ and $(\Delta v_v)_{4\text{-}6}$ (represented by $(\Delta v_h\text{-}\Delta v_v)_{4\text{-}6}$) continually increases, which indicates that the acceleration pressure drop in the horizontal elbow is higher than that in the vertical elbow. This disparity gradually increases as α_i increases.

(2) The difference in slip ratio between the two types of pipes (represented by $(\Delta S_h\text{-}\Delta S_v)_{4\text{-}6}$) continuously increases and remains positive, indicating that the frictional head loss in the horizontal elbow is greater than that in the vertical elbow. It continues to increase as α_i increases.

(3) The density difference between vertical and horizontal elbows at Surface-6 (represented by $(\rho_v\text{-}\rho_h)_6$) increases with α_i. When α_i=0.05, $(\rho_v\text{-}\rho_h)_6$ is relatively small and the weight of the acceleration pressure drop and friction pressure drop in the total pressure drop becomes greater, which results in a larger Δp in the horizontal elbow with larger head loss due to oil-gas separation in comparison to the vertical elbow. The $(\rho_v\text{-}\rho_h)_6$ value increases with α_i, signifying that the influence of gravity pressure drop is more significant than the other two types of pressure drop. Therefore, the Δp value in a vertical elbow is greater than that in a horizontal elbow when α_i=1.0-1.5.

Table 4 Parameters at inlet and outlet of elbow with different α_i

Parameters	Inlet void fraction		
	α_i = 0.05	α_i = 0.10	α_i = 0.15
$(\Delta v_h\text{-}\Delta v_v)_{4\text{-}6}$ (m/s)	0.017	0.067	0.106
$(\Delta S_h\text{-}\Delta S_v)_{4\text{-}6}$	0.041	0.138	0.171
$(\rho_v\text{-}\rho_h)_6$ (kg/m^3)	6.532	19.297	26.075

In Δp_{max}, the proportion of the gravity pressure drop is smaller than that in Δp. The void fraction and oil velocity in the straight section downstream are higher than those in the elbow, so the impact of acceleration pressure drop and friction pressure drop are more significant than those in Δp. Therefore, the Δp_{max} of a horizontal elbow is greater than that of a vertical elbow under all α_i values.

5. CONCLUSION

Numerical simulations were conducted in this study to investigate oil-gas two-phase flows in vertical and horizontal 90° elbows of an aero-engine lubrication system. The influence of asymmetric secondary-flow vortices on pressure drop were revealed by analyzing the changes in void fraction, flow rate, slip ratio, and pressure in the pipes, and then the following findings were obtained.

(1) A steady-state Euler-Euler approach CFD model was established based on the theory of homogeneous flow. The algebraic relationship of gas-liquid relative velocity is prescribed through slip velocity equation. It was found after experiment verification that the model can effectively describe the motion of lubricating oil-air bubbly flow and predict its pressure drop across 90° elbows.

(2) The phenomenon of oil-gas separation is exacerbated by a large-scale and high-gas-content vortex extending from the inside of 45° corner to the downstream of the elbow, as well as the asymmetric secondary-flow vortices caused by gravity, making the air velocity lower than the lubricating oil velocity. The separation of oil and gas caused by secondary-flow vortices not only causes additional local head loss in an elbow, but also leads to greater acceleration pressure drop.

(3) For bubbly flow, the separation of oil and gas caused by asymmetric secondary flow results in a lower density of mixture at the outlet of a horizontal elbow compared to a vertical elbow, thereby increasing the weight of gravity pressure drop in total pressure drop.

This phenomenon is further intensified with the increase in void fraction of upstream flow.

ACKNOWLEDGEMENTS

This research is supported by the Youth Science and Technology Talent "Seedling Raising" Project of the Educational Department of Liaoning Province (JYT2020116) and the project from the Key Laboratory of Power Transmission Technology on Aero-engine, Aero Engine Corporation of China (220121186a).

CONFLICT OF INTEREST

There are not conflicts to disclose.

AUTHORS CONTRIBUTION

W. Sha established the models and wrote the manuscript. **G. Leng** provided funding support and experimental data. R. S. Xu provided methodological guidance. **S. Li** assisted in proofreading the manuscript and drawing tables.

REFERENCES

Al-Safran, E., & Al-Qenae, K. (2018). A study of flow-pattern transitions in high-viscosity oil-and-gas two-phase flow in horizontal pipes. *SPE Production & Operations*, *33*(02), 269–280. https://doi.org/10.2118/187939-PA

Atif, A., & Senouci, S. (2019). Numerical analysis of performance deterioration of a centrifugal pump operating in two-phase flows. *Journal of Applied Fluid Mechanics*, *12*(4), 1203-1211. https://doi.org/10.29252/jafm.12.04.29477

Ban, S., Pao, W., & Nasif, M. S. (2018). Numerical simulation of two-phase flow regime in horizontal pipe and its validation. *International Journal of Numerical Methods for Heat & Fluid Flow*, *28*(6), 1279-1314. https://doi.org/10.1108/HFF-05-2017-0195

Bowden, R. C., Lessard, E., & Yang, S. K. (2018). Void fraction measurements of bubbly flow in a horizontal 90 degrees bend using wire mesh sensors. *International Journal of Multiphase Flow*, 99, 30-47. https://doi.org/10.1016/j.ijmultiphaseflow.2017.09.009

Bressani, M., & Mazza, R. A. (2018). Two-phase slug flow through an upward vertical to horizontal transition. *Experimental Thermal and Fluid Science*, *91*, 245-255. https://doi.org/10.1016/j.expthermflusci.2017.10.023

Chen, Q., Podila, K., Rao, Y. F., Bowden, R., & Yang, S. K. (2019). Assessment of CFD for unheated gas-liquid flows with high void fraction. *Nuclear Engineering and Design*, *341*, 346-359. https://doi.org/10.1016/j.nucengdes.2018.11.016

Chisholm, D. (1980). Two-phase flow in bends. *International Journal of Multiphase Flow*, *6*(4), 363-367. https://doi.org/10.1016/0301-9322(80)90028-2

Dang, Z. R., Yang, Z. J., Yang, X. H., & Ishii, M. (2018). Experimental study of vertical and horizontal two-phase pipe flow through double 90 degree elbows. *International Journal of Heat and Mass Transfer*, *120*, 861-869. https://doi.org/10.1016/j.ijheatmasstransfer.2017.11.089

Debnath, R., Mandal, A., Majumder, S., Bhattaeharjee, S., & Roy, D. (2015). Numerical analysis of turbulent fluid flow and heat transfer in a rectangular elbow. *Journal of Applied Fluid Mechanics*, *8*(2), 231-241. https://doi.org/10.18869/acadpub.jafm.67.221.21363

Fang, L., Wang, S., Li, S., Faraj, Y., Tian, J., & Li, X. (2020). Phase content and flow measurement of bubble flow based on new experimental pipe. *Journal of Applied Fluid Mechanics*, *13*(2), 469-478. https://doi.org/10.29252/jafm.13.02.30344

Flouros, M., Hendrick P., Outirba, B., Cottier, F., & Proestler, S. (2015). Thermal and flow phenomena associated with the behavior of brush seals in aero engine bearing chambers. *Journal of Engineering for Gas Turbines and Power-Transactions of the ASME*, *137*(9), 1-12. https://doi.org/10.1115/1.4029711

Flouros, M., Kanarachos, A., Yakinthos, K., Salpingidou, C., & Cottier, F. (2016). Two-phase flow pressure drop in corrugated tubes used in an aero-engine oil system. *Journal of Engineering for Gas Turbines and Power-Transactions of the ASME*, *138*(6), 1-22. https://doi.org/10.1115/1.4031627

Kim, H. G., & Kim, S. M. (2022). Experimental investigation of flow and pressure drop characteristics of air-oil slug flow in a horizontal tube. *International Journal of Heat and Mass Transfer*, *183*, 122063. https://doi.org/10.1016/j.ijheatmasstransfer.2021.122063

Kong, R., Qiao, S. X., Kim, S., Bajorek, S., Tien, K., & Hoxie, C. (2018). Interfacial area transport models for horizontal air-water bubbly flow in different pipe sizes. *International Journal of Multiphase Flow*, *106*, 46-59. https://doi.org/10.1016/j.ijmultiphaseflow.2018.05.009

Liu, Z. M., Liu, J., & Shen F. (2015). Simulation on flow patterns and characteristics of two-phase gas-liquid flow in a 90° bend under different gravity. *Chinese Journal of Theoretical and Applied Mechanics*, *47*(2), 223-230. https://doi.org/10.6052/0459-1879-14-264

Li, Y. J., Yu, Z. Y., Ye, Q. Y., Yang, J. X., & Hayat, S.

(2022). Analysis of pressure fluctuations for oil-gas two-phase flow in a horizontal pipe using the bubble number density equation. *Chemical Engineering Communications*, *209*(3), 351-364. https://doi.org/10.1080/00986445.2020.1869950

Ogunsesan, O. A., Hossain, M., & Droubi, M. G. (2021). Computational fluid dynamics modelling of multiphase flows in double elbow geometries. *Proceedings of the Institution of Mechanical Engineers Part E-Journal of Process Mechanical Engineering*, *235*(6), 1835-1846. https://doi.org/10.1177/09544089211021744

Pour, S. S., Mohanarangam, K., Vahaji, S., Cheung, S., & Tu, J. Y. (2018). Visualization of gas-liquid bubbly flows in a large diameter pipe with 90 bend. *Journal of Visualization*, *21*(4), 585-596. https://doi.org/10.1016/10.1007/s12650-018-0486-2

Qiao, S. X., & Kim, S. (2016). Interfacial area transport across a 90 degrees vertical-upward elbow in air-water bubbly two-phase flow. *International Journal of Multiphase Flow*, *85*, 110-122. https://doi.org/10.1016/j.ijmultiphaseflow.2016.05.015

Qiao, S. X., Mena, D., & Kim, S. (2017). Inlet effects on vertical-downward air-water two-phase flow. *Nuclear Engineering and Design*, *312*, 375-388. https://doi.org/10.1016/j.nucengdes.2016.04.033

Qiao, S. X., & Kim, S. (2018). On the prediction of two-phase pressure drop across 90 degrees vertical elbows. *International Journal of Multiphase Flow*, *109*, 242-258. https://doi.org/10.1016/j.ijmultiphaseflow.2018.08.002

Schiller, L., & Naumann, Z. A. (1935). A drag coefficient correlation. *Zeitschrift des Vereins Deutscher Ingenieure*, *77*, 318–320. https://www.researchgate.net/publication/307884096_A_drag_coefficient_correlation

Yang, H., Xue, J., Li, L., Li, X., Lin, P., & Zhu, Z. (2022). Modeling of bubbly flow using a combined volume of fluid and discrete bubble model: investigation on interphase forces. *Journal of Applied Fluid Mechanics*, *15*(3), 843-855. https://doi.org/10.47176/JAFM.15.03.33280

Yayla, S., Kamal, K., & Bayraktar, S. (2019). Numerical analysis of a two-phase flow (oil and gas) in a horizontal separator used in petroleum projects. *Journal of Applied Fluid Mechanics*, *12*(4), 1037-1045. https://doi.org/10.29252/jafm.12.04.29318

Zahedi, R., & Rad, A. B. (2022). Numerical and experimental simulation of gas-liquid two-phase flow in 90-degree elbow. *Alexandria Engineering Journal*, *61*(3), 2536-2550. https://doi.org/10.1016/j.aej.2021.07.011

Zubir, M. A., Ramli, R., & Zainon, M. Z. (2019). Determination of flow patterns in vertical upward two-phase flow channel via void fraction profile. *Journal of Applied Fluid Mechanics*, *12*(2), 474-483. https://doi.org/10.29252/jafm.12.02.28351